The Astrophysical Journal Letters, 944:L49 (12pp), 2023 February 20 https://doi.org/10.3847/2041-8213/acb549

SN 2019ewu: A Peculiar Supernova with Early Strong Carbon and Weak Oxygen Features from a New Sample of Young SN Ic Spectra

Marc Williamson[1,2], Christian Vogl[2,3], Maryam Modjaz[4], Wolfgang Kerzendorf[2,5,6], Jaladh Singhal[2], Teresa Boland[7], Jamison Burke[8], Zhihao Chen[13], Daichi Hiramatsu[8], Lluís Galbany[9,10], Estefania Padilla Gonzalez[8,11], D. Andrew Howell[8,11], Saurabh W. Jha[7], Lindsey A. Kwok[7], Curtis McCully[8], Megan Newsome[8], Craig Pellegrino[8], Jeonghee Rho[12], Giacomo Terreran[8,11], and Xiaofeng Wang[13,14]
[1] Department of Physics, New York University, New York, NY 10003, USA
[2] TARDIS Collaboration
[3] Max-Planck-Institut für Astrophysik, Karl-Schwarzschild-Straße 1, D-85748 Garching bei München, Germany
[4] Department of Astronomy, University of Virginia, Charlottesville, VA 22904, USA
[5] Department of Physics and Astronomy, Michigan State University, East Lansing, MI 48824, USA
[6] Department of Computational Mathematics, Science, and Engineering, Michigan State University, East Lansing, MI 48824, USA
[7] Department of Physics and Astronomy, Rutgers, the State University of New Jersey, USA
[8] Las Cumbres Observatory, 6740 Cortona Drive, Suite 102, Goleta, CA 93117-5575, USA
[9] Institute of Space Sciences (ICE, CSIC), Campus UAB, Carrer de Can Magrans, s/n, E-08193 Barcelona, Spain
[10] Institut d'Estudis Espacials de Catalunya (IEEC), E-08034 Barcelona, Spain
[11] Department of Physics, University of California, Santa Barbara, CA 93106-9530, USA
[12] SETI Institute, 339 N. Bernardo Avenue, Suite 200, Mountain View, CA 94043, USA; jrho@seti.org
[13] Physics Department and Tsinghua Center for Astrophysics, Tsinghua University, Beijing, 100084, People's Republic of China
[14] Beijing Planetarium, Beijing Academy of Sciences and Technology, Beijing, 100044, People's Republic of China
Received 2022 November 7; revised 2023 January 3; accepted 2023 January 4; published 2023 February 22

Abstract

With the advent of high-cadence, all-sky automated surveys, supernovae (SNe) are now discovered closer than ever to their dates of explosion. However, young premaximum light follow-up spectra of Type Ic SNe (SNe Ic), probably arising from the most-stripped massive stars, remain rare despite their importance. In this Letter, we present a set of 49 optical spectra observed with the Las Cumbres Observatory through the Global Supernova Project for 6 SNe Ic, including a total of 17 premaximum spectra, of which 8 are observed more than a week before *V*-band maximum light. This data set increases the total number of publicly available premaximum-light SN Ic spectra by 25%, and we provide publicly available SNID templates that will significantly aid in the fast identification of young SNe Ic in the future. We present a detailed analysis of these spectra, including Fe II 5169 velocity measurements, O I 7774 line strengths, and continuum shapes. We compare our results to published samples of stripped SNe in the literature and find one SN in our sample that stands out. SN 2019ewu has a unique combination of features for an SN Ic: an extremely blue continuum, high absorption velocities, a P Cygni–shaped feature almost 2 weeks before maximum light that TARDIS radiative transfer modeling attributes to C II rather than Hα, and weak or nonexistent O I 7774 absorption feature until maximum light.

Unified Astronomy Thesaurus concepts: Type Ic supernovae (1730); Core-collapse supernovae (304); Radiative transfer simulations (1967); Spectroscopy (1558); Optical astronomy (1776)

Supporting material: data behind figures

1. Introduction

Stripped-envelope (SE) supernovae (SNe) whose photospheric optical spectra lack both hydrogen and helium absorption features (SNe Ic; Filippenko et al. 1993; Modjaz et al. 2019) are the explosions of massive stars that have lost their outermost layers (Clocchiatti et al. 1997), either through strong winds (Yoon 2017), binary interactions (Dessart et al. 2020; Woosley et al. 2021), or both. The spectral diversity within the SN Ic class is well documented (Liu et al. 2016; Williamson et al. 2019) and indicative of a variety of different progenitor systems, mass-loss histories, and explosion mechanics contributing to SN Ic events. For example, a subset of high-velocity SNe Ic with broad lines (SNe Ic-bl) is the only type of SN observed in conjunction with gamma-ray bursts (Modjaz et al. 2016). In the last two decades, a handful of SN Ic and SESNe sample studies have yielded valuable insights into this important SN class. For example, it has been shown that SNe Ic have stronger oxygen features than other SESN subclasses (Matheson et al. 2001; Liu et al. 2016; Fremling et al. 2018). SNe Ic also have systematically higher velocities than their helium-rich counterparts SNe Ib (Liu et al. 2016; Fremling et al. 2018). While SNe Ic are supposedly helium free, there has been much debate over potential helium contribution in well-observed SNe Ic (e.g., 1994I; Williamson et al. 2021, 2020oi; Rho et al. 2021), and a recent sample of near-infrared (NIR) SN Ic spectra covering the unblended 2 μm line shows clear evidence of weak helium features in some SNe Ic (Shahbandeh et al. 2022). These sample studies use spectral data sets that mostly cover SN Ic evolution near and after the date of maximum brightness due to the difficulty of discovering SNe soon after explosion with low-cadence surveys. The Berkeley sample of 888 SESN spectra collected over three decades by the Lick Observatory Supernova Search (LOSS;

Shivvers et al. 2018) contains only 16 SN Ic spectra that were taken before maximum light. The Palomar Transient Factory (PTF) and intermediate PTF (iPTF) SESN data set of 507 spectra (Fremling et al. 2018) contains only 46 premaximum SN Ic spectra, most of which are not yet publicly available. A set of 156 SESN spectra released by the Public ESO Spectroscopic Survey of Transient Objects (PESSTO; Smartt et al. 2015) contains only 16 premaximum SN Ic spectra (Prentice et al. 2019). The largest publicly available data set of young SN Ic spectra contains 65 premaximum (relative to *V*-band) spectra from 18 SNe Ic (hereafter the Modjaz Group Sample (MGS); Modjaz et al. 2014; Liu et al. 2016, 2017; Williamson et al. 2019). The MGS includes SESNe from the sample collected by the Harvard-Smithsonian Center for Astrophysics (CfA; Modjaz et al. 2014), SNe Ic individually published by both the Berkeley and PTF/iPTF samples, as well as individual SNe Ic spectra published in the literature, up to 2019 (Williamson et al. 2019).

The relative lack of young SN Ic spectra is a source of major uncertainty when it comes to connecting progenitor models to these explosions. Young SN Ic spectra taken only days after explosion (i.e., 1–2 weeks before *V*-band maximum light) give the most direct constraints on the outermost layers of the SN ejecta. At these phases, the photosphere (and therefore the line-forming region above it) is located far out in the ejecta, and lines are less contaminated by lower-velocity ejecta material. Therefore, young SN Ic spectra may offer the possibility of detecting early weak signatures of hydrogen or helium before these features are lost due to line blending, cooling of the ejecta, decreasing density, or a combination of these effects as the SN evolves. In addition, young SN Ic spectra offer the possibility of detecting narrow emission from flash ionization due to shock breakout (flash spectroscopy; Gal-Yam et al. 2014; Kochanek 2019; Modjaz et al. 2019). Young SN Ic spectra are also crucial for making confident classifications fast enough for other follow-up to be triggered by or before maximum light. This is particularly important for space-based ultraviolet (UV) spectroscopy using the Hubble Space Telescope (HST). SN Ic UV spectra at early times constrain the heavy-metal content of the outer layers of the ejecta (e.g., Ashall et al. 2019), yielding information on mixing during the progenitor's evolution and explosion. In addition, similar to SNe Ia (Mazzali 2000), SN Ic optical spectra are strongly influenced by high UV opacity due to heavy-metal lines. Without templates for young SN Ic spectra, misclassifications can lead to the inadvertent follow-up of the wrong SN type (e.g., SN 2021yja; Vasylyev et al. 2022). Young SN Ic spectra in the nearby universe will prove necessary for identifying high-redshift SNe Ic, where time dilation means observed spectra will be significantly younger in the SN rest frame. In addition, simulations in preparation for the Nancy Grace Roman Space Telescope (ROMAN) show that we can expect to find $\sim$3000 SNe Ia between $0.4 \leqslant z \leqslant 1.7$ (Hounsell et al. 2018), and optical SN Ic spectra will help identify potential contaminants of young SNe Ia.

Two recently discovered SNe Ic (SN 2017ein; Kilpatrick et al. 2018; Van Dyk et al. 2018, SN 2020oi; Rho et al. 2021; Gagliano et al. 2022) have demonstrated the importance of young spectra for capturing peculiar behavior within the SN Ic class. SN 2017ein exhibited abnormally strong C II features at early times for an SN Ic and shared many other spectroscopic properties with SN 2007gr (Valenti et al. 2008), the first so-called carbon-rich SN Ic (Mazzali et al. 2010). Young spectra for both SN 2017ein and SN 2007gr show clear O I 7774 typical of SNe Ic (Liu et al. 2016; Fremling et al. 2018). Similarly, SN 2020oi also shows signs of early C II, but a spectrum observed just 3 days after explosion shows surprisingly weak O I 7774 for an SN Ic (Gagliano et al. 2022). Carbon and oxygen features are particularly important for understanding SNe Ic because they can provide links to progenitor models. Dessart et al. (2012) have shown that models with higher ejecta mixing produce stronger and faster O I 7774 features, and recent stellar evolution simulations up to shock breakout have shown that a binary companion causes increased carbon yield in core-collapse SNe (Farmer et al. 2021; Laplace et al. 2021).

In this Letter, we address the scarcity of young SN Ic spectra and present detailed modeling of the most peculiar object, SN 2019ewu. We present a publicly available data set of 49 SN Ic spectra from 6 different events, including 17 premaximum-light spectra in Section 2. We discuss our analysis methodology in Section 3 including how we correct for extinction, calculate spectral phases, characterize line velocity and strength, quantify continuum shape, and\ model SN 2019ewu. In Section 4 we present our results and compare the new SNe Ic in this paper to previous large samples from the literature (e.g., the MGS, PTF/iPTF Sample, Berkeley Sample). We show that SN 2019ewu exhibits unique early C II features for SNe Ic (both in strength and shape) as well as anomalously weak O I 7774. While a handful of SNe Ic in the literature have shown somewhat similar early carbon features, SN 2019ewu is the only SN Ic to exhibit such a weak O I 7774 absorption up to maximum light. We present models for SN 2019ewu using the radiative transfer code TARDIS (Kerzendorf & Sim 2014; Kerzendorf et al. 2022) in Section 4.5 and conclude in Section 5.

2. Observations

We present a data set of 49 spectra from 6 different SNe Ic obtained through the LCO (Brown et al. 2013) collaboration between 2019 January and 2021 July as part of the Global Supernova Project (GSP). As part of the selection criteria, we choose SNe Ic with spectral time series that includes at least one premaximum-light spectrum (relative to the *V* band). The data set presented here includes a total of 17 premaximum SN Ic spectra, which is an increase of 25% to the number of publicly available young SN Ic spectra. Table 1 shows a summary of the data set.

All six SNe presented here were eventually classified as SNe Ic, but some showed similarities to other SN types at early times. SN 2019cda was discovered (Leonini 2019) by the Italian Supernovae Search Project (ISSP) and initially classified as Type SN Ic using SuperFit (Hiramatsu et al. 2019b). SN 2019ewu was discovered (Tonry et al. 2019) by the ATLAS group and initially classified as Type SN II due to a blue continuum and the appearance of a broad feature that was interpreted as Hα (Hiramatsu et al. 2019a). SN 2019yz was discovered (Fremling 2019) by ZTF and initially classified as Type SN Ic using SuperFit (Burke et al. 2019). SN 2020akf was discovered (Tonry et al. 2020) by the ATLAS group and initially classified as Type SN Ia using SuperFit (Burke et al. 2020). SN 2021mxx was discovered (Forster et al. 2021) by ZTF and initially classified as Type SN Ia by SuperFit (Pellegrino et al. 2021). Finally, SN 2021do was discovered (Fremling 2021) by ZTF and initially classified as Type SN Ic

Table 1
Summary of SN Spectra

SN Name	SN Type[a]	z	$t_{V_{max}}$(MJD)	Phases[b]
SN 2019cda	Ic	0.027652	58575.9	−7.3, −6.5, 0.5, 7.3
SN 2019ewu	Ic	0.033	58625.4	−11.6, −4.9, 0.0, 9.7, 15.5, 28.0
SN 2019yz	Ic	0.00639	58516.2	−8.6, −7.6, 28.1, 38.1, 41.5, 46.0, 54.0, 61.9, 69.9, 82.7, 93.7
SN 2020akf	Ic	0.012	58883.8	−13.1, −12.2, −10.9, −4.4, −0.4, 27.2, 44.9, 57.9, 65.8, 73.6, 83.5, 94.4, 109.2, 125.9
SN 2021mxx	Ic	0.00965	59365.1	−7.6, −6.5, −4.7, −3.6, −0.7, 7.2, 14.3, 24.2, 33.1, 43.9, 61.7
SN 2021do	Ic	0.009346	59227.2	−0.7, 3.2, 27.9

Notes.
[a] SNe are classified by running SNID with the most updated SESNe template library (Liu et al. 2016; Modjaz et al. 2016; Williamson et al. 2019).
[b] Phases are rounded to the nearest tenth and are in the rest frame, relative to the date of V-band maximum. The date of the peak in the available bands is fit with the Monte Carlo method of Bianco et al. (2014) and if V-band data are not available, the date of the peak is converted to the V band using the empirical relations from Bianco et al. (2014). SNEX V-band photometry is used for SN 2019ewu and SN 2020akf, while LASAIR (Smith et al. 2019) r-band photometry is used for the remaining objects.

(Voziakova et al. 2021). Here we reclassify SN 2019ewu, SN 2020akf, and SN 2021mxx as SNe Ic based on their spectra at maximum light using SNID and the MGS template libraries. We note that half of the young SNe Ic in this sample were initially misclassified most likely due to a lack of early template spectra in the libraries of codes like SNID.

Table 2 details the observation log for each spectrum included. Optical spectra were taken using the FLOYDS spectrographs on the 2 m telescopes at Siding Spring Observatory (COJ 2m) and Haleakala (OGG 2m). FLOYDS spectra cover the wavelength range from 3500 to 10000 Å at a resolution varying between $400 \leqslant R \leqslant 700$. We include one spectrum for SN 2020akf that was shared with the GSP and was observed by the Beijing Faint Object Spectrograph and Camera (BFOSC) using a 2.16 m telescope (2.16BAO) covering a slightly narrower optical wavelength range at a similar resolution of $500 \leqslant R \leqslant 2000$ (Fan et al. 2016).

3. Methodology

In this section, we discuss the choices made to process and analyze the SN Ic spectra in our data set. This includes extinction correction, classification, phase calculation, and spectral feature and continuum shape characterization. The spectra are extracted from raw images using the FLOYDS Pipeline,[15] which includes cosmic-ray cleaning, trace extraction, and wavelength and flux calibration.

3.1. Extinction Correction

For each SN, we calculate the Milky Way (MW) extinction using Schlafly & Finkbeiner (2011) via the NASA/IPAC calculator.[16] MW extinction corrections are made assuming $R_V = 3.1$ and a Fitzpatrick (1999) reddening law for consistency with the methodology used by Barbarino et al. (2021) to analyze the SNe Ic from the Palomar Transient Factory (PTF; Law et al. 2009; Rau et al. 2009). Table 3 shows the positions of the SNe in our data set on the sky and their associated MW extinction correction. We note that SN 2019yz and SN 2021do show narrow Na I D absorption features at rest at their host-galaxy redshifts, but we do not correct for host-galaxy extinction due to relatively large uncertainties (i.e., 0.2 mag in $E(B-V)$ reported in Poznanski et al. 2012) associated with methods correlating the Na I feature strength with extinction.

3.2. Spectrum Phases and Peak Calculation

Each SN in our data set has observed photometry that covers the lightcurve peak in at least one band, so spectral phases are calculated relative to the date of maximum. Specifically, the date of maximum is calculated for the V band either directly or using the conversion factor for the appropriate band (Bianco et al. 2014) for consistency with the analysis of the MGS, one of the largest publicly available spectral data sets of SNe Ic. The date of maximum light is calculated using a Monte Carlo process to fit a quadratic around the lightcurve peak (Bianco et al. 2014). LCO V-band photometry is used for SN 2019ewu and SN 2020akf, and ZTF (Bellm et al. 2018) r-band difference photometry obtained using the LASAIR (Smith et al. 2019) broker is used for the remaining SNe and the date of maximum converted to the V band. We note that the conversion of the date of the r-band to the V-band peak involves an uncertainty of $\sim$1 day. Table 1 shows the dates of maximum in the V band ($t_{V_{max}}$) calculated in MJD for each of the SNe in our data set.

3.3. Spectral Classification

We use the Supernova Identification code (SNID; Blondin & Tonry 2007) to classify the spectra in our data set. SNID works by cross-correlating the newly observed spectra in our data set with a library of previously observed and typed SN spectral templates. In order to obtain robust classifications from SNID, it is imperative to use the most updated template libraries. In this case, we use the stripped-SN templates from the MGS. For each SN in our sample, we run SNID on the spectrum closest to the date of maximum (i.e., $t_{V_{max}} = 0$ days) to produce a robust classification. In addition, we run SNID on the earliest spectrum for each SN in order to check for consistency with initial classification attempts and to identify SNe with uncertain or evolving early types. We focus discussion on the three SNe in this sample that were originally classified as types other than SN Ic (SN 2019ewu, SN 2020akf, and SN 2021mxx).

3.4. Line Strengths and Velocities

Line strengths and velocities are important quantitative tools for understanding SN spectra in the context of previously observed SN samples and for understanding SN dynamics and

[15] https://lco.global/documentation/data/floyds-pipeline/
[16] https://irsa.ipac.caltech.edu/applications/DUST/

Table 2
Spectra Observation Log

SN ($t_{V_{max}}$ days)	Telescope	Instrument	Exposure (s)	Slit (arcsec)	Airmass
2019cda (−7.3)	OGG 2m	FLOYDS	3600	2″	1.25
2019cda (−6.5)	OGG 2m	FLOYDS	3600	2″	1.26
2019cda (0.5)	OGG 2m	FLOYDS	3600	2″	1.28
2019cda (7.3)	OGG 2m	FLOYDS	3600	2″	1.25
2019ewu (−11.6)	OGG 2m	FLOYDS	3600	2″	1.38
2019ewu (−4.9)	OGG 2m	FLOYDS	3600	2″	1.21
2019ewu (0.0)	OGG 2m	FLOYDS	3600	2″	1.46
2019ewu (9.7)	OGG 2m	FLOYDS	3600	2″	1.41
2019ewu (15.5)	OGG 2m	FLOYDS	3600	2″	1.42
2019ewu (28.0)	OGG 2m	FLOYDS	3600	2″	1.31
2019yz (−8.6)	OGG 2m	FLOYDS	2700	2″	1.74
2019yz (−7.6)	OGG 2m	FLOYDS	2700	2″	1.52
2019yz (28.1)	OGG 2m	FLOYDS	2700	2″	1.50
2019yz (38.1)	OGG 2m	FLOYDS	2700	2″	1.14
2019yz (41.5)	SALT	RSS	2194	1.5″	1.26
2019yz (46.0)	OGG 2m	FLOYDS	3600	2″	1.08
2019yz (54.0)	OGG 2m	FLOYDS	3600	2″	1.08
2019yz (61.9)	OGG 2m	FLOYDS	3600	2″	1.09
2019yz (69.9)	COJ 2m	FLOYDS	3600	2″	1.40
2019yz (82.7)	OGG 2m	FLOYDS	3600	2″	1.09
2019yz (93.7)	COJ 2m	FLOYDS	3600	2″	1.20
2020akf (−13.1)	OGG 2m	FLOYDS	3600	2″	1.35
2020akf (−12.2)	OGG 2m	FLOYDS	3599	2″	1.06
2020akf (−10.9)	2.16/BAO	BFOSC	3600	2.3″	1.01
2020akf (−4.4)	OGG 2m	FLOYDS	2700	2″	1.36
2020akf (−0.4)	OGG 2m	FLOYDS	2700	2″	1.17
2020akf (27.2)	OGG 2m	FLOYDS	2700	2″	1.06
2020akf (44.9)	OGG 2m	FLOYDS	3600	2″	1.14
2020akf (57.9)	OGG 2m	FLOYDS	2700	2″	1.21
2020akf (65.8)	OGG 2m	FLOYDS	2699	2″	1.42
2020akf (73.6)	OGG 2m	FLOYDS	2700	2″	1.14
2020akf (83.5)	OGG 2m	FLOYDS	2700	2″	1.17
2020akf (94.4)	OGG 2m	FLOYDS	3599	2″	1.39
2020akf (109.2)	OGG 2m	FLOYDS	3600	2″	1.47
2020akf (125.9)	OGG 2m	FLOYDS	3600	2″	1.73
2021mxx (−7.6)	OGG 2m	FLOYDS	2700	2″	1.38
2021mxx (−6.5)	OGG 2m	FLOYDS	2700	2″	1.07
2021mxx (−4.7)	OGG 2m	FLOYDS	2699	2″	1.44
2021mxx (−3.6)	COJ 2m	FLOYDS	2700	2″	1.07
2021mxx (−0.7)	OGG 2m	FLOYDS	2700	2″	1.36
2021mxx (7.2)	COJ 2m	FLOYDS	1800	2″	1.34
2021mxx (14.3)	COJ 2m	FLOYDS	1800	2″	1.05
2021mxx (24.2)	COJ 2m	FLOYDS	1800	2″	1.15
2021mxx (33.1)	COJ 2m	FLOYDS	2700	2″	1.28
2021mxx (43.9)	COJ 2m	FLOYDS	2700	2″	1.08
2021mxx (61.7)	COJ 2m	FLOYDS	2699	2″	1.08
2021do (−0.7)	OGG 2m	FLOYDS	2699	2″	1.71
2021do (3.2)	OGG 2m	FLOYDS	2700	2″	1.69
2021do (27.9)	OGG 2m	FLOYDS	3600	2″	1.70

their progenitors. In order to include uncertainties in our reported line velocities and strengths, we first calculate uncertainty arrays for each SN spectrum in our data set using the Fourier smoothing method developed by Liu et al. (2016). We use these uncertainty arrays instead of the uncertainty arrays directly from the reduction for a consistent comparison of the uncertainties of our line velocities and strengths to those from the MGS. It has been shown that the Fourier-derived uncertainty arrays do not introduce systematic uncertainties (see Figure 17; Liu et al. 2016). We calculate uncertainties for line velocities and strengths by resampling the spectra in our data set hundreds of times using the uncertainty arrays to generate Gaussian noise in each wavelength bin. Line velocities and strengths are then calculated for each resampled spectrum to characterize the uncertainty in each calculation.

Line velocities are found by fitting a quadratic around the absorption minimum to identify a wavelength shift relative to the rest wavelength of a given line (e.g., Blondin et al. 2006;

Table 3
Extinction

SN	R.A. (h m s)	Decl. (° ' ")	$E(B-V)_{MW}$[a] (mag)
19cda	10:44:49.84	+06:36:04.0	0.03
19ewu	13:17:12.25	+53:54:57.4	0.02
19yz[b]	15:41:57.30	+00:42:39.4	0.10
20akf	09:28:39.62	+38:33:47.1	0.01
21mxx	18:56:51.27	+36:37:20.4	0.08
21do[b]	10:16:56.67	+73:23:51.3	0.02

Notes.
[a] Milky Way extinction is calculated using Schlafly & Finkbeiner (2011).
[b] Host-galaxy extinction is evident from the presence of a narrow Na I D line at the host-galaxy redshift. In this case, host extinction is calculated using Equation (1) from Taubenberger et al. (2006). See the discussion in Section 3.1.

Liu et al. 2016). This wavelength shift is converted to a velocity using the relativistic Doppler shift. In this work, we focus on the Fe II 5169 line because it has previously been used as a tracer of the photospheric velocity in stripped-envelope SNe (Liu et al. 2016; Modjaz et al. 2016; Barbarino et al. 2021). We note that robust line velocities strongly depend on confident line identification, which can be difficult for core-collapse SNe, which can exhibit high degrees of line blending due to high ejecta velocities, especially at early times. For this reason, we restrict ourselves to calculating the Fe II 5169 line velocities to spectra where the characteristic "W" Fe doublet feature is clearly visible.

We use the pseudo-equivalent width (pEW; Blondin et al. 2011; Silverman et al. 2012; Liu et al. 2016) to quantify line strengths and particularly focus on the O I 7774 line for our SN Ic data set. The O I 7774 line is relatively easy to identify (i.e., unblended), appears even in very early SN Ic spectra, and has been reported in previous SN Ic sample studies (Matheson et al. 2001; Liu et al. 2016; Barbarino et al. 2021). Furthermore, oxygen (the most abundant heavy element in the universe) may be tied to the progenitor structure. For example, some simulations have shown that lower-mass progenitors produce smaller oxygen buffer regions between the inner and outer layers of SN ejecta, affecting nonthermal excitation that is crucial for SESNe (Dessart et al. 2012). In addition, progenitors with similar core masses at the time of collapse from binaries versus single-star systems show systematic differences in carbon and oxygen structure (Laplace et al. 2021). To calculate the O I 7774 pEW, we follow the methodology of Liu et al. (2016), which is summarized below. Local maxima on either side of the O I 7774 absorption minimum are identified, and the local continuum is defined as a line connecting those points. The pEW is calculated using Equation (1) from Liu et al. (2016).

3.5. Characterizing Young SN Ic Continua

In order to quantify the diverse continuum behavior exhibited by the SNe Ic in our data set (particularly at early times), we calculate the color evolution directly from the spectra using the ST-mag system[17] used by HST. The ST-mag system is defined such that an object with constant flux per unit wavelength has zero color, so it is easily interpretable. We use the standard Bessell bands[18] (Bessell & Murphy 2012) and the open-source package WSYNPHOT[19] to calculate magnitudes and colors directly from spectra. It has been shown that calculating colors directly from SESN spectra without absolute calibration to photometry introduces only a minor uncertainty of ∼0.15 mag for phases before 20 days postmaximum light (see Figure 10; Modjaz et al. 2014).

3.6. Spectral Modeling with TARDIS

In order to robustly identify lines in blended spectra, radiative transfer simulations are required. TARDIS is a fast, 1D, open-source radiative transfer code for modeling SN spectra. TARDIS has been used to model a wide variety of SN types, including SNe Ic. In particular, TARDIS includes a nonlocal thermodynamic equilibrium (NLTE) approximation for the ionization and excitation treatment of helium (Boyle et al. 2017), which is important for modeling stripped-envelope SNe. In this paper, we use two different versions of TARDIS to model the earliest spectrum of SN 2019ewu, which contains an absorption feature that could potentially be attributed to hydrogen (see Section 4.4). The public[20] version of TARDIS (v2022.06.19) currently does not include the continuum processes necessary for an accurate treatment of H (work is ongoing to incorporate the physics from Vogl et al. 2019, which will include continuum processes in the public TARDIS). We therefore use the public TARDIS in order to establish a baseline model without H and to attempt to explain the SN 2019ewu absorption feature using C or Si. Our models assume a power-law density profile $\rho = \rho_0(v/v_0)^n$, where the parameters are chosen to be consistent with the hydrodynamical simulations of an exploded stripped star (Iwamoto et al. 1994) that have been used for radiative transfer simulations of SN Ic 1994I (Hachinger et al. 2012; Williamson et al. 2021). We keep the exponent $n = -6.78$ fixed (fit from the outer layers of the hydrodynamical simulation) but vary the normalization parameter ρ_0 to experiment with different ejecta masses. We assume the date of explosion to be on 2019 May 7 according to the last nondetection (Tonry et al. 2019) because TARDIS requires a parameter for the time since explosion. We note that due to the assumption of homologous expansion, there is a degeneracy between the time since explosion and density profile parameters. Our primary focus with the models therefore is to understand the elements causing line formation in the ejecta.

We use the nonpublic version of TARDIS presented in Vogl et al. (2019), which includes continuum processes and has been used to model H-rich SNe IIP (Vogl et al. 2020; Vasylyev et al. 2022) to modify the baseline model by adding H to the ejecta. We do not use the consistent thermal balancing implemented by Vogl et al. (2020) since it ignores some heating and cooling processes for species other than H and He, which might make it unreliable for a hydrogen-poor SN. We instead follow the standard coupling of electron temperature to radiative temperature $T_e = 0.9T_{rad}$ (Mazzali & Lucy 1993). The nonpublic version of TARDIS also includes an NLTE treatment for the ionization and excitation states of H.

[17] https://hst-docs.stsci.edu/acsdhb
[18] http://svo2.cab.inta-csic.es/theory/fps/index.php
[19] https://github.com/starkit/wsynphot
[20] https://github.com/tardis-sn/tardis

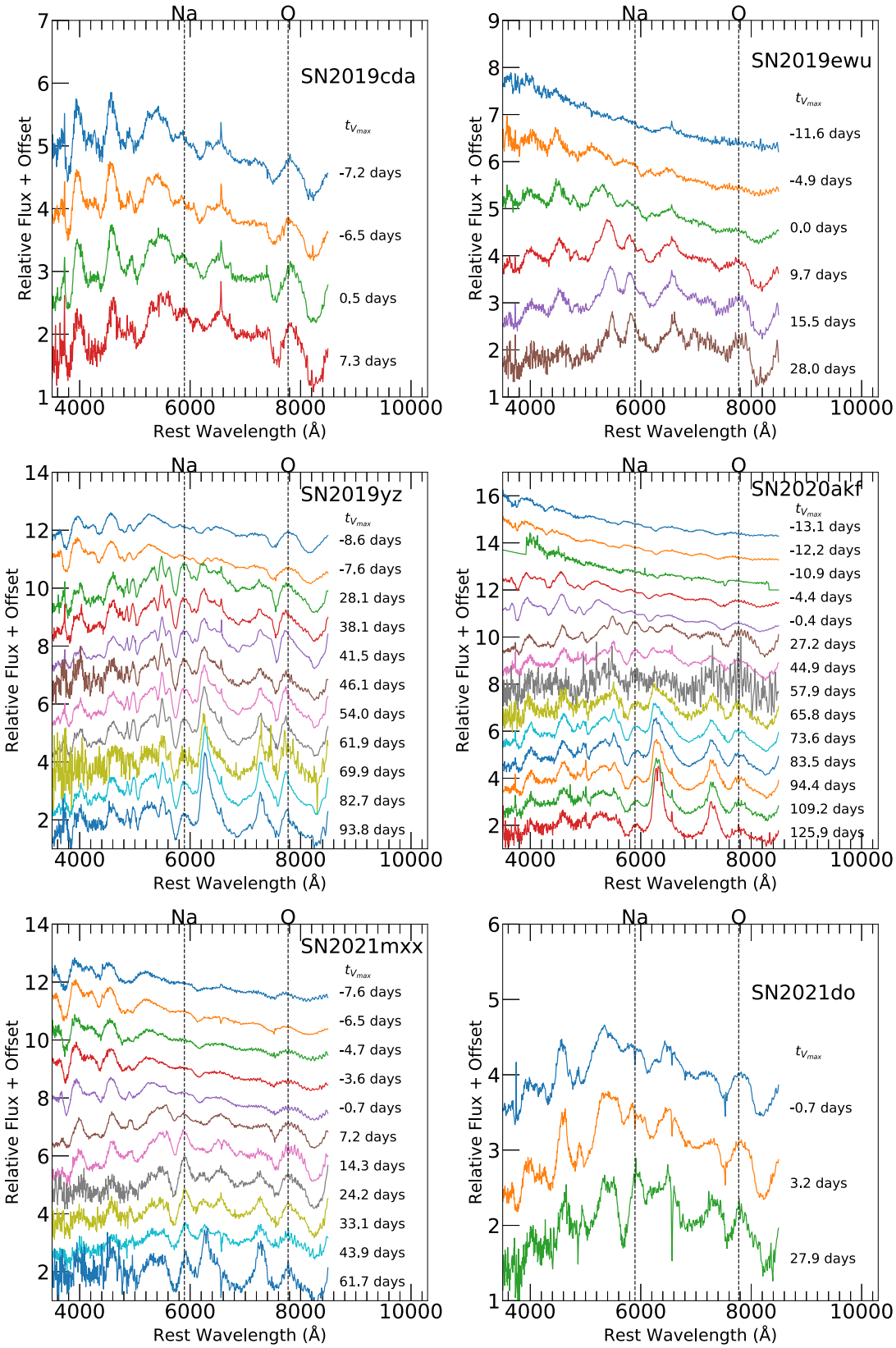

Figure 1. Spectral time series for the six SNe Ic analyzed in this work (corrected for MW but not host-galaxy extinction). Dashed vertical lines mark the Na 5896 and O 7774 lines, and phases are relative to the date of the *V*-band maximum. All SNe with the exception of SN 2021do were discovered early enough to obtain spectra more than 1 week prior to maximum light. We note that SN 2019ewu and SN 2020akf have blue featureless spectra at very early times for SNe Ic, which may be related to their slow-developing and weak O 7774 feature compared to the other SNe.

4. Results

Figure 1 shows the spectral time series of the SNe Ic in our data set. The spectra shown are corrected for extinction as discussed in Section 3.1, and each spectrum is labeled with the phase relative to the *V*-band maximum as discussed in Section 3.2. The O I 7774 line is marked with a dashed vertical line to highlight the diversity in behavior observed in this wavelength region among the SNe. For example, SN 2019ewu shows no evidence (or very weak evidence) for an O I 7774 feature premaximum while SN 2019yz shows strong evidence for O I 7774 even more than a week before the *V*-band maximum. We also mark the Na I D line (5893 Å) with a dashed vertical line to highlight the major contaminant for He I 5876 discussed for SNe Ic.

4.1. Classifying Young SN Ic Spectra

Robustly classifying SN spectra as early as possible is crucial for identifying targets appropriate for follow-up observations (i.e., NIR or UV spectroscopy), particularly if follow-up takes time to schedule (i.e., ∼1 week for HST). In addition, science cases may require follow-up at or before the SN reaches maximum light. However, classifying young SN spectra is particularly challenging due to the scarcity of similarly young previously observed data. Template-matching classification codes (e.g., SNID; Blondin & Tonry 2007, SuperFit; Howell et al. 2005) require previously observed young spectral templates of the same type in order to make robust classifications, and machine-learning-based algorithms (e.g., SESNPCA; Williamson et al. 2019, DASH; Muthukrishna et al. 2019) require young training spectra. The MGS contains 23 SNe Ic and 259 spectra with $t_{V_{\max}} < 60$ days, but only 15 spectra have $t_{V_{\max}} < -7$ days. The GSP SN Ic sample presented in this paper includes eight new spectra with $t_{V_{\max}} < -7$ days and increases the total number of premaximum-light spectra by 25%. SNID templates for the SNe Ic presented in this paper are publicly available.[21]

Three of the six SNe Ic presented in this paper were initially misclassified using their earliest spectra. SN 2019ewu was classified as SN II due to the potential Hα P Cygni profile and blue continuum. SN 2020akf and SN 2021mxx were initially misclassified as SNe Ia due to the relatively strong potential Si II absorption along with the characteristic lack of H and He features. Using the SESN SNID templates from the current MGS, we find good spectral matches for these young misclassified spectra to a variety of stripped-SN types. SN 2021mxx matches multiple typical SNe Ic including SN 2007cl and SN 2004dn. We find good spectral matches for SN 2020akf to two stripped superluminous SNe (SLSNe Ic), iPTF13ajg (Vreeswijk et al. 2014) and SSS120810-23 (Nicholl et al. 2014). As shown by Liu et al. (2017), SLSNe Ic and SNe Ic-bl exhibit similar velocities, and these matches reflect the high line velocities exhibited in SN 2020akf spectra that are discussed further in Section 4.2. In addition, SN 2020akf exhibits a "W"-shaped feature at early times near λ4300 that is attributed to O II in SLSNe Ic and absent in SNe Ic (Quimby et al. 2011; Gal-Yam 2012; Nicholl et al. 2015; Mazzali et al. 2016; Liu et al. 2017).

SN 2019ewu is particularly interesting because it is the only SN Ic in the sample presented here that is misclassified as a H-rich SN II at early times. Figure 2 shows a subset of the spectral time series for SN 2019ewu including spectral matches for each phase (colors). At $t_{V_{\max}} = -12$ days, SNID identifies the typical SN IIP 1999em as a good spectral match to SN 2019ewu due to the P Cygni–shaped feature near 6200 Å. As SN 2019ewu evolved, it more clearly became a stripped SN, though its high velocities yield best matches those of SNe Ic-bl as it approached peak before matching with more typical SNe Ic at $t_{V_{\max}} \geqslant 0$.

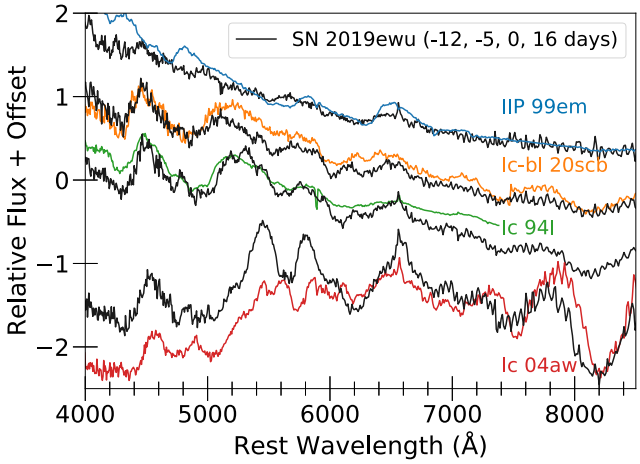

Figure 2. A subset of the SN 2019ewu spectral time series (black) at −12, −5, 0, and 16 days relative to the *V*-band maximum. Colored spectra show particularly good spectral matches identified by SNID at each phase. SN 2019ewu initially matches with SN II before developing broad lines typical of SN Ic-bl, before settling as an SN Ic.

4.2. High-velocity SNe Ic and the Connection to SNe Ic-bl

SNe Ic-bl spectra have two distinguishing features compared to normal SNe Ic: extremely broad lines and systematically higher absorption velocities (Modjaz et al. 2016). However, previous sample studies of SNe Ic and Ic-bl spectra have identified a handful of outliers that appear to bridge these two classes. PTF12gzk is an SN Ic with typical narrow features but with high absorption velocities more consistent with SNe Ic-bl associated with gamma-ray bursts (Ben-Ami et al. 2012; Modjaz et al. 2016). PTF2009dh was classified as SN Ic-bl due to early broad lines (Prentice et al. 2016) but was reclassified as a normal SN Ic (Barbarino et al. 2021). Sample studies of SN Ic spectra measuring the absorption velocity of the Fe II 5169 line have shown that on average premaximum ejecta velocities are approximately 12,000 km s^{-1} and rarely exceed 15,000 km s^{-1} (Modjaz et al. 2016; Barbarino et al. 2021). However, Modjaz et al. (2016) identify SN Ic 2004aw with extremely high premaximum velocities closer to 20,000 km s^{-1}, consistent with some SNe Ic-bl without associated GRBs (Taubenberger et al. 2006). Likewise for PTF10bip, Modjaz et al. (2020) concluded it was unclear whether the SN was Ic or Ic-bl due to the high velocities and blending they saw in the PTF spectra, and Barbarino et al. (2021) also concluded anomalously high Fe II 5169 velocity from the same PTF spectra, which are not publicly available for comparison. Figure 3 shows the Fe II 5169 absorption velocity for the GSP SN Ic sample presented in this paper (colors) compared to the average velocity of the MGS (gray band). We find that the velocities of our sample are mostly consistent with those of the MGS with the exception of SN 2019ewu, which exhibits abnormally high velocities,

[21] https://github.com/nyusngroup/SESNtemple

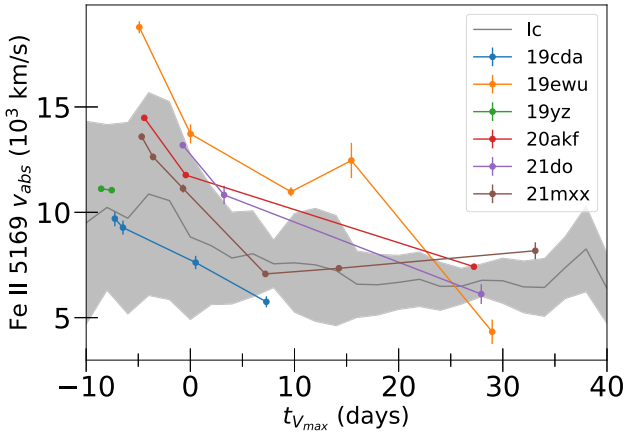

Figure 3. Fe II 5169 absorption velocities measured as a function of $t_{V_{max}}$ for the GSP SN Ic sample (colored lines) compared to the mean ±1 standard deviation velocity of the SN Ic sample from Liu et al. (2016) shown as the gray band. Velocities are calculated only when Fe II 5169 can be clearly identified from the Fe doublet. A clear identification of Fe II 5169 cannot be made for SN 2019yz after early times due to contamination from an emergent feature.

(The data used to create this figure are available.)

particularly at early times ($t_{V_{max}} < 0$) where $v_{abs} = 18,000$ km s^{-1}. In fact, early spectra of SN 2019ewu match with SN Ic-bl 2020scb (see Figure 2) and SN 2004aw. High-velocity SNe Ic like SN 2019ewu may provide clues to the relationship between normal SNe Ic and SNe Ic-bl.

4.3. Continuum Shape and Feature Strength

Figure 1 highlights the spectral diversity of the GSP SN Ic sample presented in this work. In particular, two aspects of the premaximum ($t_{V_{max}} < 0$) spectra are noteworthy: feature strength and continuum shape. The left panel of Figure 4 shows the O I 7774 pEW as a function of time for the GSP SN Ic sample (colors) compared to the MGS (gray). Modjaz et al. (2016) and Fremling et al. (2018) both showed that SN Ic spectra have O I 7774 pEW in the range of 60–80 Å at all phases, including before maximum light. However, we find that SN 2019ewu (already an outlier for its anomalously high velocities discussed in Section 4.2) is also a strong outlier in this regard. We find the earliest spectrum ($t_{V_{max}} = -12$ days) does not have an identifiable O I 7774 feature, and when this feature does appear a week later, the pEW is less than 25 Å. This gives SN 2019ewu the weakest O I 7774 feature of all the SNe Ic analyzed in the MGS. The PTF SN Ic sample does have two SNe Ic with similarly weak O I 7774 early features (see top panel of Figure 3; Fremling et al. 2018), but these SNe are not identified in the paper, and the data behind the figure are not publicly available. The abnormally weak early O I 7774 feature in SN 2019ewu makes it an exception to the general trend first noted by Matheson et al. (2001) that SNe Ic have stronger oxygen features than SNe Ib. By $t_{V_{max}} \approx 20$ days, the O I 7774 feature in SN 2019ewu has evolved to be consistent with the SN Ic class, highlighting the importance of early spectra for discovering new behavior in SNe Ic.

The right panel of Figure 4 shows the $B-V$ colors using the ST-mag system calculated directly from the GSP SN Ic spectra. We use these colors to evaluate the diversity of spectral continuum shapes observed within our sample but note that the spectra are not corrected for host-galaxy extinction. For colors calculated directly from spectra for SESNe with $t_{V_{max}} < 20$ days, there is a typical uncertainty of ∼0.15 mag (Modjaz et al. 2014), which cannot explain the range of colors observed in our sample. This uncertainty increases to ∼0.37 mag after $t_{V_{max}} > 20$ days, which may explain some of the oscillations that appear to be present in the color curves. SN 2019ewu distinguishes itself again from the majority of the SNe Ic in this sample with a particularly blue early continuum. We note that SN 2019ewu (orange) shows an extremely similar continuum shape to SN 2020akf (red), but while SN 2019ewu exhibits relatively featureless early spectra, SN 2020akf shows typical early O I 7774 absorption with pEW ≈80 Å. Therefore, a simple photospheric temperature difference is unlikely to explain the difference between the O I 7774 pEW strengths for these two SNe. More detailed radiative transfer modeling is required to investigate the differences between SN 2019ewu and SN 2020akf. Early blue relatively featureless continua have also been observed in some standard SNe Ic-bl (SN 2014ad; Kwok et al. 2022) as well as more exotic SNe Ic-bl (SN 2018gep; Pritchard et al. 2021, iPTF16asu; Taddia et al.

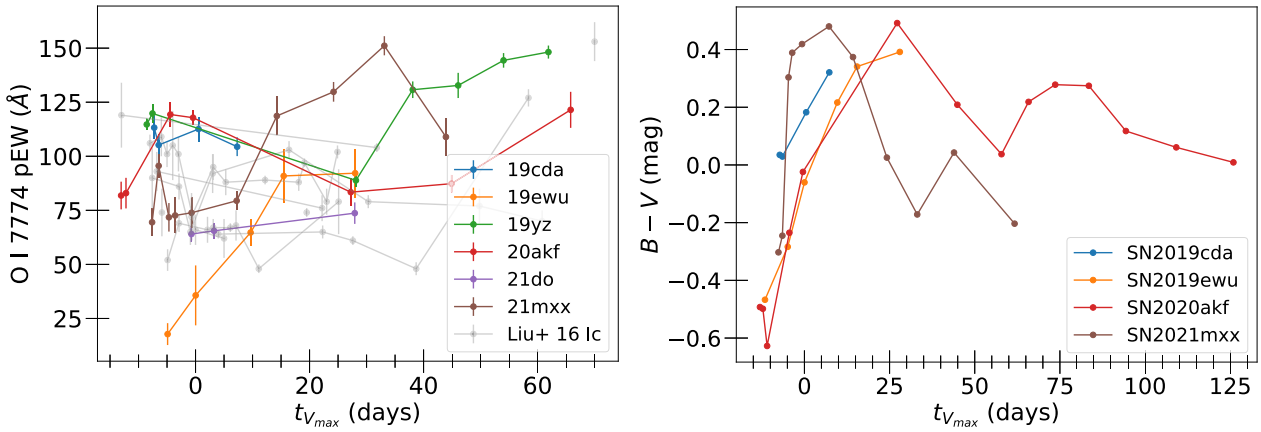

Figure 4. (Left) The O I 7774 absorption line pseudo-equivalent width (pEW) as a function of time for the GSP SN Ic sample (colors) compared to the distribution of SNe Ic from the MGS (gray). SN 2019ewu has particularly weak oxygen absorption at early times. (Right) ($B-V$) colors calculated directly from the GSP spectra using the ST-mag system. All spectra are dereddened to correct for MW extinction but may be contaminated by host-galaxy extinction. SN 2019yz and SN 2021do are excluded because their spectra show narrow Na I D lines indicative of host-galaxy extinction. SN 2019ewu and SN 2020akf show particularly blue early-time spectra but different oxygen line strengths.

(The data used to create this figure are available.)

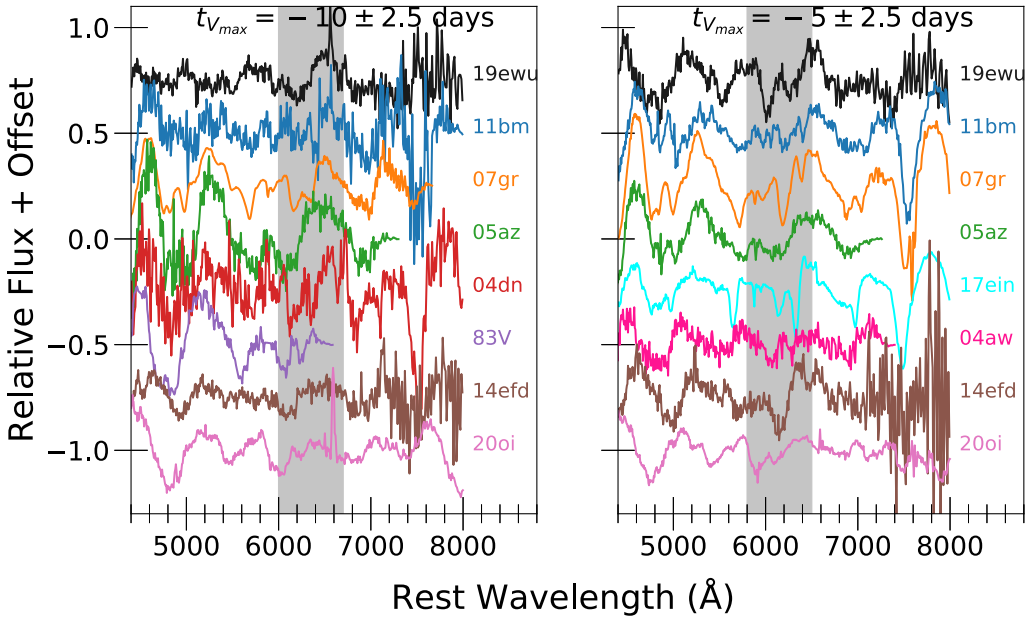

Figure 5. A comparison of the first two spectra of SN 2019ewu (black) to SNe Ic from the MGS at a similar phase relative to the *V*-band maximum (colors), as well as spectra from SN Ic 2020oi (Rho et al. 2021). The spectra shown here are continuum removed by SNID to facilitate line-shape comparison. The left figure highlights the broad P Cygni feature in SN 2019ewu that has not been seen before in early-time SN Ic spectra, while the right figure shows how the feature evolves one week later to develop a doublet shape.

2019), both of which are connected to the new class of Fast Blue Optical Transients (FBOTs; Inserra 2019). We note that the blue continuum exhibited by SN 2019ewu and SN 2020akf is also seen in the recently observed SN Ic 2022oqm (Irani et al. 2022).

4.4. Comparing SN 2019ewu to Other SNe Ic

SN 2019ewu is noteworthy as an SN Ic for its high velocities (see Section 4.2) and early blue continuum with weak oxygen features (see Section 4.3). In addition, one of its most puzzling characteristics is a similarity to SN II spectra at early times (see Section 4.1). Figure 5 shows a comparison of the earliest two SN 2019ewu spectra to SN Ic spectra at similar phases from the MGS as well as the recently discovered SN Ic 2020oi (Rho et al. 2021; Gagliano et al. 2022), which had particularly early spectral follow-up. In the left panel, the shaded region highlights that SN 2019ewu is the only SN Ic to show such a strong, clearly sinusoidal feature in the shaded region. This P Cygni–shaped feature coincides with the location for Hα absorption and emission at 6563 Å, which explains the SNID template matches to SN II spectra. However, SN 2019ewu does not exhibit any feature that could correspond to Hβ. A similar absorption feature seen in SN 2007gr is attributed to C II (Valenti et al. 2008), but SN 2007gr does not exhibit the emission or P Cygni shape of the feature observed in SN 2019ewu. We note some similarities between SN 2005az, which was originally classified as both SN Ib and SN Ic (Aldering et al. 2005; Quimby et al. 2005), but the emission part of the feature is too broad compared to SN 2019ewu. NIR spectra could help identify carbon lines (e.g., SN 2020oi; Rho et al. 2021, 2021krf; Ravi et al. 2022), but no NIR spectra were obtained for SN 2019ewu.

The right panel of Figure 5 shows a spectral comparison for the subsequent SN 2019ewu spectrum a week later, where the broad P Cygni feature has developed a doublet shape. We note that the evolution of SN 2019ewu in this respect is dramatically different from SN 2005az. The doublet feature shown in SN 2019ewu is seen in SN 2004aw to a weaker degree and possibly in SN 2007gr with a slower velocity structure. SN 2020oi also exhibits this doublet feature, but with slightly broader and weaker lines. Both SN 2004aw and SN 2007gr attribute this doublet feature to Si II λ6355 and C II λ6580 (Taubenberger et al. 2006; Valenti et al. 2008). SN 2007gr appears to be the best analog to SN 2019ewu for the feature highlighted in the shaded region of Figure 5. We note that Figure 5 highlights the difference in O I 7774 feature strength. SN 2019ewu shows no O I 7774 in its earliest spectrum and a much weaker feature a week later, in stark contrast to the pronounced O I 7774 feature in other carbon-rich SNe Ic, SN 2007gr and SN 2017ein. SN 2022oqm also appears to show a similarly shaped C II absorption/emission feature early in its evolution that also evolves into a doublet attributed to carbon and silicon (see Figure 2 Irani et al. 2022). However, there is a clear, broad, O I 7774 absorption feature in the SN 2022oqm SEDM spectrum +6.46 days after explosion (which corresponds to ~1 week before *V*-band maximum). SN 2019ewu is unique in having a combination of early carbon and a lack of O I 7774 absorption until $t_{V_{max}} = 0$.

4.5. TARDIS Models for SN 2019ewu

Radiative transfer modeling is required in order to better understand the earliest spectrum ($t_{V_{max}} = -12$ days) of SN 2019ewu. It is particularly important to explain the P Cygni–shaped feature highlighted in the shaded region of the left panel of Figure 5 because this could be evidence of hydrogen. There has been some discussion in the literature of hydrogen potentially contributing to the spectral features of SN Ic 1994I (Hachinger et al. 2012; Parrent et al. 2016), but there has not been a confident identification of hydrogen features in an SN Ic backed by modeling. The prevailing theory is that SNe Ic progenitors are highly stripped due to binary interactions (Podsiadlowski et al. 1992; Yoon 2015) or strong

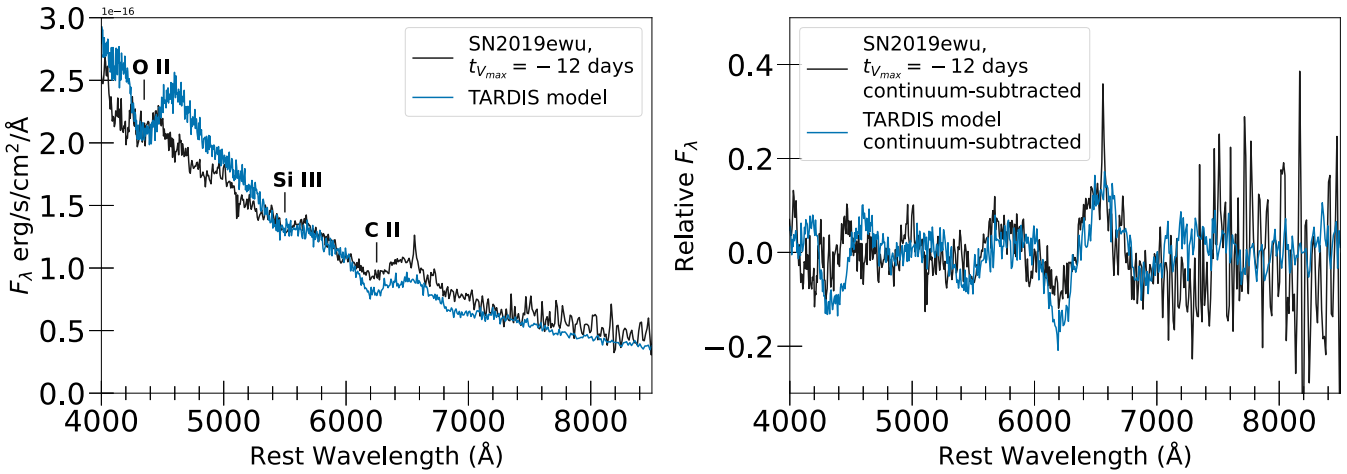

Figure 6. (Left) A TARDIS model (blue) for the first spectrum of SN 2019ewu (black). The primary features of the model are labeled (O II, Si III, C II). (Right) A comparison of the model and observed spectrum from the left panel with continuum removed by SNID to highlight the ability of the model to reproduce the lines seen in the data. The P Cygni–shaped feature in the SN 2019ewu spectrum can be produced in the model without any hydrogen.

winds from massive single stars (Crowther 2007; Smartt 2009) such that they have lost their hydrogen envelopes (Schneider et al. 2021; Woosley et al. 2021).

Figure 6 shows the results of modeling the earliest spectrum of SN 2019ewu with the public version of TARDIS. The model assumes uniform abundances from elements typical of SNe Ic (Dessart et al. 2015; Williamson et al. 2021) including (He, C, N, O, Ne, Na, Mg, Si, S, Ca, and Fe-group elements). In particular, the model shown in Figure 6 has a carbon abundance fraction of $\chi_C = 0.35$ and does not include any hydrogen. The TARDIS model file is publicly available.[22] The left panel of Figure 6 shows that the TARDIS model (in blue) is overall a very good match to the data, although very slightly too blue, a difference that could be explained by a moderate amount of host extinction for SN 2019ewu. The right panel of Figure 6 shows a comparison between SN 2019ewu and the model flattened by SNID to better compare the lines. The model reproduces the observed features in SN 2019ewu very well, including the P Cygni–shaped feature. This model does not include any hydrogen, and tracking the photon packet interactions from the simulation shows that more than 90% of the absorption in the λ6200 feature is due to C II. Combined with the lack of observed Hβ feature in the SN 2019ewu spectrum, we conclude that the P Cygni–shaped feature at λ6200 is most likely due to C II. In order to check whether hydrogen could contribute significantly to this feature, we have run a grid of simulations with the nonpublic TARDIS version from Vogl et al. (2019) which allows a more accurate treatment of hydrogen-rich SNe. We modified the baseline TARDIS model from Figure 6 to include a variety of hydrogen abundances up to 30%. The results of these simulations (run including continuum processes and an NLTE treatment for H) show that the hydrogen contribution to the ∼6200 Å feature is negligible compared to C II for the adopted composition and range of photospheric temperatures investigated. This is true even when H fractional abundance is increased to 30%. In summary, we can be confident that the P Cygni profile seen in the −12 day spectrum of SN 2019ewu, even though it appears at wavelengths where SNe II show Hα and even though SNID matches the SN 2019ewu spectrum with those of hydrogen-rich SNe, is not due to Hα, but can be explained by C II.

[22] https://github.com/tardis-sn/tardis-setups/tree/master/2022/williamson_19ewu

5. Summary

In this paper, we present a data set of 49 spectra from 6 SNe Ic including a total of 17 spectra observed before the *V*-band maximum. This data set is publicly available and increases the number of available premaximum SN Ic spectra in the MGS by 25%. These young spectra are critical to include as either templates or training data for SN spectral classifiers so that robust classifications can be made closer to the date of explosion. This in turn will facilitate faster follow-up observations (e.g., HST UV spectroscopy) with less chance that an object has been misclassified (e.g., SN 2021yja; Vasylyev et al. 2022). In addition, extremely young spectra like the one observed for SN 2019ewu ($t_{V_{max}} = -12$ days) can provide important information on the outermost layers of the ejecta for SNe Ic, yielding constraints on stripping mechanisms and progenitor models. In particular, we note that oxygen abundance in the ejecta has been tied to pre-explosion progenitor core mass (Dessart et al. 2012), and recent work indicates that carbon and oxygen abundance gradients in the ejecta differ depending on whether the progenitor system is a massive single star versus a binary system (Farmer et al. 2021; Laplace et al. 2021). We conduct a thorough analysis of the spectra presented here, including calculating Fe II 5169 velocities, O I 7774 feature strengths, and $B - V$ colors. We also compare this new sample of SNe Ic to publicly available data sets like the MGS (Modjaz et al. 2014; Liu et al. 2016; Williamson et al. 2019), PTF/iPTF sample (Fremling et al. 2018), and the CSP sample (Shahbandeh et al. 2022). We find that by all metrics, SN 2019ewu is an outlier SN Ic. SN 2019ewu exhibits extremely high ejecta velocities consistent with some SN Ic-bl spectra, while also displaying extremely weak O I 7774 features. SN 2019ewu is therefore a counterexample to the general trend that SNe Ic have stronger O I 7774 features than SNe Ib (Matheson et al. 2001). We show that SN 2019ewu exhibits peculiar early-time behavior including a very blue continuum and a P Cygni–shaped feature near λ6200 that evolves into a strong doublet a week later. Our extensive modeling efforts identify C II as the primary source of the early P Cygni feature and not Hα. We therefore add

SN 2019ewu to a growing subset of SNe Ic that exhibit particularly strong early carbon features. These carbon-rich SNe Ic may be connected to the higher carbon yields derived from binary progenitor systems studied by Farmer et al. (2021) and warrant further study. Specifically, modeling of the entire SN 2019ewu spectral time series is called for to investigate the development of the strong doublet feature discussed in Section 4.4 and to understand the abnormally weak early oxygen features.

We are grateful to the anonymous referee for quick and insightful comments. This work makes use of data from the Las Cumbres Observatory network of telescopes. The LCO group is supported by NSF grants AST-1911225 and AST-1911151. This work was supported in part through the NYU IT High Performance Computing resources, services, and staff expertise. Marc Williamson is supported by the NASA Future Investigators in NASA Earth and Space Science and Technology grant (80NSSC21K1849). C.V. was supported for part of this work by the Excellence Cluster ORIGINS, which is funded by the Deutsche Forschungsgemeinschaft (DFG, German Research Foundation) under Germany's Excellence Strategy-EXC-2094-390783311.

M.M. acknowledges support in part from NASA under Swift GI program 1619152 (NASA grant No. 80NSSC21K0280), Tess GI program G03267 (NASA grant No. 80NSSC21K0240), ADAP program grant No. 80NSSC22K0486, HST GO program HST-GO-16178.007, and teaching relief from a 19 Washington Square North Award.

This research made use of TARDIS, a community-developed software package for spectral synthesis in supernovae (Kerzendorf & Sim 2014; Kerzendorf et al. 2022). The development of TARDIS received support from GitHub, the Google Summer of Code initiative, and ESA's Summer of Code in Space program. TARDIS is a fiscally sponsored project of NumFOCUS. TARDIS makes extensive use of Astropy and Pyne. Based on observations obtained with the Samuel Oschin 48-inch Telescope at the Palomar Observatory as part of the Zwicky Transient Facility project. ZTF is supported by the National Science Foundation under grant No. AST-1440341 and grant No. AST-2034437 and a collaboration including Caltech, IPAC, the Weizmann Institute for Science, the Oskar Klein Center at Stockholm University, the University of Maryland, the University of Washington, Deutsches Elektronen-Synchrotron and Humboldt University, Los Alamos National Laboratories, the TANGO Consortium of Taiwan, the University of Wisconsin at Milwaukee, and Lawrence Berkeley National Laboratories, Trinity College Dublin, and IN2P3, France. Operations are conducted by COO, IPAC, and UW.

L.G. acknowledges financial support from the Spanish Ministerio de Ciencia e Innovación (MCIN), the Agencia Estatal de Investigación (AEI) 10.13039/501100011033, and the European Social Fund (ESF) "Investing in your future" under the 2019 Ramón y Cajal program RYC2019-027683-I and the PID2020-115253GA-I00 HOSTFLOWS project, from Centro Superior de Investigaciones Científicas (CSIC) under the PIE project 20215AT016, and the program Unidad de Excelencia María de Maeztu CEX2020-001058-M.

ORCID iDs

Marc Williamson https://orcid.org/0000-0003-2544-4516
Christian Vogl https://orcid.org/0000-0002-7941-5692
Maryam Modjaz https://orcid.org/0000-0001-7132-0333
Wolfgang Kerzendorf https://orcid.org/0000-0002-0479-7235
Jaladh Singhal https://orcid.org/0000-0002-8310-0829
Jamison Burke https://orcid.org/0000-0003-0035-6659
Zhihao Chen https://orcid.org/0000-0001-5175-4652
Daichi Hiramatsu https://orcid.org/0000-0002-1125-9187
Lluís Galbany https://orcid.org/0000-0002-1296-6887
Estefania Padilla Gonzalez https://orcid.org/0000-0003-0209-9246
D. Andrew Howell https://orcid.org/0000-0003-4253-656X
Saurabh W. Jha https://orcid.org/0000-0001-8738-6011
Lindsey A. Kwok https://orcid.org/0000-0003-3108-1328
Curtis McCully https://orcid.org/0000-0001-5807-7893
Craig Pellegrino https://orcid.org/0000-0002-7472-1279
Jeonghee Rho https://orcid.org/0000-0003-3643-839X
Giacomo Terreran https://orcid.org/0000-0003-0794-5982
Xiaofeng Wang https://orcid.org/0000-0002-7334-2357

References

Aldering, G., Lee, B. C., Loken, S., et al. 2005, ATel, 451, 1
Ashall, C., Mazzali, P. A., Pian, E., et al. 2019, MNRAS, 487, 5824
Barbarino, C., Sollerman, J., Taddia, F., et al. 2021, A&A, 651, A81
Bellm, E. C., Kulkarni, S. R., Graham, M. J., et al. 2018, PASP, 131, 018002
Ben-Ami, S., Gal-Yam, A., Filippenko, A. V., et al. 2012, ApJL, 760, L33
Bessell, M., & Murphy, S. 2012, PASP, 124, 140
Bianco, F. B., Modjaz, M., Hicken, M., et al. 2014, ApJS, 213, 19
Blondin, S., Mandel, K. S., & Kirshner, R. P. 2011, A&A, 526, A81
Blondin, S., & Tonry, J. L. 2007, ApJ, 666, 1024
Blondin, S., Dessart, L., Leibundgut, B., et al. 2006, AJ, 131, 1648
Boyle, A., Sim, S. A., Hachinger, S., & Kerzendorf, W. 2017, A&A, 599, A46
Brown, T. M., Baliber, N., Bianco, F. B., et al. 2013, PASP, 125, 1031
Burke, J., Arcavi, I., Hiramatsu, D., et al. 2019, TNSCR, 2019-1232, 1
Burke, J., Arcavi, I., Hiramatsu, D., et al. 2020, TNSCR, 2020-241, 1
Clocchiatti, A., Wheeler, J. C., Phillips, M. M., et al. 1997, ApJ, 483, 675
Crowther, P. A. 2007, ARA&A, 45, 177
Dessart, L., Hillier, D. J., Li, C., & Woosley, S. 2012, MNRAS, 424, 2139
Dessart, L., Hillier, D. J., Woosley, S., et al. 2015, MNRAS, 453, 2189
Dessart, L., Yoon, S.-C., Aguilera-Dena, D. R., & Langer, N. 2020, A&A, 642, A106
Fan, Z., Wang, H., Jiang, X., et al. 2016, PASP, 128, 115005
Farmer, R., Laplace, E., de Mink, S. E., & Justham, S. 2021, ApJ, 923, 214
Filippenko, A. V., Matheson, T., & Ho, L. C. 1993, ApJ, 415, L103
Fitzpatrick, E. L. 1999, PASP, 111, 63
Forster, F., Munoz-Arancibia, A., Bauer, F. E., et al. 2021, TNSTR, 2021-17521, 1
Fremling, C. 2019, TNSTR, 2019-131, 1
Fremling, C. 2021, TNSTR, 2021-33, 1
Fremling, C., Sollerman, J., Kasliwal, M., et al. 2018, A&A, 618, A37
Gagliano, A., Izzo, L., Kilpatrick, C. D., et al. 2022, ApJ, 924, 55
Gal-Yam, A. 2012, Sci, 337, 927
Gal-Yam, A., Arcavi, I., Ofek, E. O., et al. 2014, Natur, 509, 471
Hachinger, S., Mazzali, P. A., Taubenberger, S., et al. 2012, MNRAS, 422, 70
Hiramatsu, D., Burke, J., Arcavi, I., et al. 2019a, TNSCR, 2019-745, 1
Hiramatsu, D., Howell, D. A., Arcavi, I., et al. 2019b, TNSCR, 2019-445, 1
Hounsell, R., Scolnic, D., Foley, R. J., et al. 2018, ApJ, 867, 23
Howell, D. A., Sullivan, M., Perrett, K., et al. 2005, ApJ, 634, 1190
Inserra, C. 2019, NatAs, 3, 697
Irani, I., Chen, P., Morag, J., et al. 2022, arXiv:2210.02554
Iwamoto, K., Nomoto, K., Höflich, P., et al. 1994, ApJL, 437, L115
Kerzendorf, W., Sim, S., Vogl, C., et al. 2022, tardis-sn/tardis: TARDIS v2022.06.19, Zenodo, doi:10.5281/zenodo.6662839
Kerzendorf, W. E., & Sim, S. A. 2014, MNRAS, 440, 387
Kilpatrick, C. D., Takaro, T., Foley, R. J., et al. 2018, MNRAS, 480, 2072
Kochanek, C. S. 2019, MNRAS, 483, 3762
Kwok, L. A., Williamson, M., Jha, S. W., et al. 2022, ApJ, 937, 40
Laplace, E., Justham, S., Renzo, M., et al. 2021, A&A, 656, A58
Law, N. M., Kulkarni, S. R., Dekany, R. G., et al. 2009, PASP, 121, 1395
Leonini, S. 2019, TNSCR, 2019-434, 1
Liu, Y.-Q., Modjaz, M., & Bianco, F. B. 2017, ApJ, 845, 85
Liu, Y.-Q., Modjaz, M., Bianco, F. B., & Graur, O. 2016, ApJ, 827, 90

Matheson, T., Filippenko, A. V., Li, W., Leonard, D. C., & Shields, J. C. 2001, AJ, 121, 1648
Mazzali, P., & Lucy, L. 1993, A&A, 279, 447
Mazzali, P. A., Sullivan, M., Pian, E., Greiner, J., & Kann, D. A. 2016, MNRAS, 458, 3455
Mazzali, P. A. 2000, A&A, 363, 705
Mazzali, P. A., Maurer, I., Valenti, S., Kotak, R., & Hunter, D. 2010, MNRAS, 408, 87
Modjaz, M., Gutierrez, C. P., & Arcavi, I. 2019, NatAs, 3, 717
Modjaz, M., Liu, Y. Q., Bianco, F. B., & Graur, O. 2016, ApJ, 832, 108
Modjaz, M., Blondin, S., Kirshner, R. P., et al. 2014, AJ, 147, 99
Modjaz, M., Bianco, F. B., Siwek, M., et al. 2020, ApJ, 892, 153
Muthukrishna, D., Parkinson, D., & Tucker, B. E. 2019, ApJ, 885, 85
Nicholl, M., Smartt, S. J., Jerkstrand, A., et al. 2014, MNRAS, 444, 2096
Nicholl, M., Smartt, S. J., Jerkstrand, A., et al. 2015, MNRAS, 452, 3869
Parrent, J. T., Milisavljevic, D., Soderberg, A. M., & Parthasarathy, M. 2016, ApJ, 820, 75
Pellegrino, C., Hiramatsu, D., Burke, J., et al. 2021, TNSCR, 2021-1794, 1
Podsiadlowski, P., Joss, P. C., & Hsu, J. J. L. 1992, ApJ, 391, 246
Poznanski, D., Prochaska, J. X., & Bloom, J. S. 2012, MNRAS, 426, 1465
Prentice, S. J., Mazzali, P. A., Pian, E., et al. 2016, MNRAS, 458, 2973
Prentice, S. J., Ashall, C., James, P. A., et al. 2019, MNRAS, 485, 1559
Pritchard, T. A., Bensch, K., Modjaz, M., et al. 2021, ApJ, 915, 121
Quimby, R., Mondol, P., Hoeflich, P., Wheeler, J. C., & Gerardy, C. 2005, IAUC, 8503, 1
Quimby, R. M., Kulkarni, S. R., Kasliwal, M. M., et al. 2011, Natur, 474, 487
Rau, A., Kulkarni, S. R., Law, N. M., et al. 2009, PASP, 121, 1334
Ravi, A. P., Rho, J., Park, S., et al. 2022, arXiv:2211.00205
Rho, J., Evans, A., Geballe, T. R., et al. 2021, ApJ, 908, 232
Schlafly, E. F., & Finkbeiner, D. P. 2011, ApJ, 737, 103
Schneider, F. R. N., Podsiadlowski, P., & Müller, B. 2021, A&A, 645, A5
Shahbandeh, M., Hsiao, E. Y., Ashall, C., et al. 2022, ApJ, 925, 175
Shivvers, I., Filippenko, A. V., Silverman, J. M., et al. 2018, MNRAS, 482, 1545
Silverman, J. M., Kong, J. J., & Filippenko, A. V. 2012, MNRAS, 425, 1819
Smartt, S. J. 2009, ARA&A, 47, 63
Smartt, S. J., Valenti, S., Fraser, M., et al. 2015, A&A, 579, A40
Smith, K. W., Williams, R. D., Young, D. R., et al. 2019, RNAAS, 3, 26
Taddia, F., Sollerman, J., Fremling, C., et al. 2019, A&A, 621, A71
Taubenberger, S., Pastorello, A., Mazzali, P. A., et al. 2006, MNRAS, 371, 1459
Tonry, J., Denneau, L., Heinze, A., et al. 2019, TNSTR, 2019-735, 1
Tonry, J., Denneau, L., Heinze, A., et al. 2020, TNSTR, 2020-206, 1
Valenti, S., Elias-Rosa, N., Taubenberger, S., et al. 2008, ApJ, 673, L155
Van Dyk, S. D., Zheng, W., Brink, T. G., et al. 2018, ApJ, 860, 90
Vasylyev, S. S., Filippenko, A. V., Vogl, C., et al. 2022, ApJ, 934, 134
Vogl, C., Kerzendorf, W. E., Sim, S. A., et al. 2020, A&A, 633, A88
Vogl, C., Sim, S. A., Noebauer, U. M., Kerzendorf, W. E., & Hillebrandt, W. 2019, A&A, 621, A29
Voziakova, O., Lander, S., Dodin, A., et al. 2021, TNSCR, 2021-51, 1
Vreeswijk, P. M., Savaglio, S., Gal-Yam, A., et al. 2014, ApJ, 797, 24
Williamson, M., Kerzendorf, W., & Modjaz, M. 2021, ApJ, 908, 150
Williamson, M., Modjaz, M., & Bianco, F. B. 2019, ApJL, 880, L22
Woosley, S., Sukhbold, T., & Kasen, D. 2021, ApJ, 913, 145
Yoon, S.-C. 2015, PASA, 32, e015
Yoon, S.-C. 2017, MNRAS, 470, 3970